

ON THE TORQUE REVERSALS OF ACCRETING NEUTRON STARS

Ünal Ertan [★]

Sabancı University, 34956, Orhanlı Tuzla, İstanbul, Turkey

Accepted XXX. Received YYY; in original form ZZZ

ABSTRACT

We have extended the analytical model proposed earlier to estimate the inner disk radius of accreting neutron stars in the strong-propeller (SP) phase, and the conditions for the transitions between the strong and weak propeller (WP) phases (Ertan 2017, 2018) to the WP (accretion with spin-down) and the spin-up (SU) phases, and the torque reversals during the WP/SU transitions. The model can account for some basic observed properties of these systems that are not expected in conventional models: (1) accretion on to the star at low X-ray luminosities and the transitions to the SP phase (no accretion) at critical accretion rates much lower than the rate required for the spin-up/spin-down transition, (2) ongoing accretion throughout a large range of accretion rates while the source is spinning down (WP phase), and (3) transitions between the spin-up and spin-down phases with comparable torque magnitudes, without substantial changes in the mass-flow rate. Our results indicate that the magnitudes of the torques on either side of the torque reversal have a ratio similar for different systems independently of their spin periods, magnetic dipole moments and accretion rates during the transitions. Estimated torque reversal properties in our model are in agreement with the observed torque reversals of 4U 1626–67.

Key words: pulsars: individual (4U 1626–67) – accretion – accretion disks

1 INTRODUCTION

Neutron stars interacting with accretion disks have three different regimes depending on the mass inflow rate \dot{M}_{in} : (1) at the lowest \dot{M}_{in} a strong-propeller regime in which no mass accretion on to the star takes place and the neutron star is spinning down, (2) at intermediate \dot{M}_{in} a weak propeller regime (accretion with spin-down) in which most or part of the matter is accreted on to the star, and the star is spinning down, and (3) at the highest \dot{M}_{in} , a spin-up regime in which all of the matter flowing in from the outer disk is accreted on to star. The critical values of \dot{M}_{in} where the transitions between these different regimes take place and the corresponding locations of the inner disk radius r_{in} depend on the magnetic dipole moment μ and the rotation rate Ω_s of the neutron star. Recently, Ertan (2017, 2018) showed that r_{in} does not track, and is much smaller than the conventional Alfvén radius, r_A , and has a weak dependence on \dot{M}_{in} in the strong-propeller phase. In this model, r_{in} tracks the co-rotation radius, r_{co} , where the closed field lines rotate with the Kepler speed, in the weak-propeller phase.

This understanding of the transitions between the strong and the weak propeller regimes is successful in explaining the properties and torque variation of transitional millisecond pulsars (tMSPs) during their transitions between the radio pulsar and the X-ray pulsar

states (Archibald et al. 2009, Papitto et al. 2013, Bassa et al. 2014, Jaodand et al. 2016). In these systems, the accretion on to the star persists at X-ray luminosities much lower than the critical spin-up/spin-down transition level (Papitto et al. 2015, Archibald et al. 2015) estimated in the conventional models (Illarionov & Sunyaev 1975, Ghosh & Lamb 1979). Hereafter, we will denote the weak-propeller, strong-propeller and spin-up phases by "WP", "SP", and "SU" respectively.

While the properties of tMSPs constrain the models for the SP/WP transitions, a few strongly magnetized ($\mu > 10^{29}$ G cm³) accreting pulsars in LMXBs with relatively long spin periods provide laboratories to study the transitions between the WP and SU phases, that is, torque reversals. Among these LMXBs, 4U 1626–67 (Chakrabarty et al. 1997a), Her X-1, (Deeter et al. 1989, Wilson et al. 1994), GX 1+4 (Chakrabarty et al. 1997b) showed torque reversals, transitions between the SU and WP phases. Some X-ray pulsars in high mass X-ray binaries (HMXBs) also show torque reversals (Bildsten et al. 1997, İnam et al. 2009). Nevertheless, HMXBs are not very convenient to study the details of the disk-field interaction due to the effect of the wind from the companion. Among the LMXBs that show spin-up/spin-down transitions, GX 1+4 (Hinkle et al. 2006) is also thought to accrete from the wind of its companion possibly with transient disk formation (Camero-Arranz et al. 2010). Her X-1 has a persistent disk, but varying attenuation of the pulsar due to near edge-on view does not allow a detailed study of

[★] E-mail: unal@sabaciuniv.edu

its X-ray luminosity and the torque relation (Pettersen et al. 1991). 4U 1626–67 seems to be the best source to study the details of the disk-field interaction leading to observed torque reversals, while similarities in the torque reversal properties of other LMXBs, and possibly HMXBs with disk-fed neutron stars could also give hints for the mechanism of these transitions.

There are several common, striking properties of LMXBs showing torque reversals which are not addressed by the conventional models (see Bildsten et al. 1997 for a review): (1) the magnitudes of the torques before and after the torque reversal are similar, (2) the accretion on to the star goes on while the star is spinning down, (3) torque reversals do not require a significant change in the mass accretion rate. In this work, to explain these basic properties of neutron stars interacting with geometrically thin accretion disks, we extend the model developed earlier by Ertan (2017, 2018) to include the SP, WP and SU phases, and the transitions between these phases in a single picture. We will test our model results with the torque reversal properties of 4U 1626–67, and also give the results for illustrative model sources with different periods and magnetic dipole moments. In Section 2, we describe the details of the model. In Section 3, we discuss our results with examples and comparisons with the observations of 4U 1626–67. Our conclusions are summarized in Section 4.

2 THE MODEL

Conventional Alfvén radius, r_A is calculated by equating the magnetic pressure of the dipole field of the neutron star to the ram pressure of matter accreting with spherical symmetry on to the neutron star, which gives $r_A \simeq (GM)^{1/7} \mu^{4/7} \dot{M}^{-2/7}$ (Davidson & Ostriker 1973, Lamb et al. 1973) where G is the gravitational constant, M and μ are the mass and magnetic dipole moment of the neutron star, and \dot{M} is the mass accretion rate. The conditions in the case of accretion from a geometrically thin disk are rather different from the spherical accretion. At a given radius r , the disk matter moves with Kepler speed, $v_K = r\Omega_K$, with a mass density orders of magnitude greater than in the spherical accretion at a given radius. Furthermore, the radial speed of matter in the disk is orders of magnitude smaller than in the spherical accretion. Despite these differences, the radius at which the magnetic and viscous stresses are balanced in the disk accretion is estimated to be very close to r_A within a factor of 2 (Ghosh & Lamb 1979, Arons 1993, Ostriker & Shu 1995, Wang 1998). Hereafter, we denote this radius by $r_\xi = \xi r_A$, and in our calculations we set $\xi = 0.5$ as estimated by Ghosh & Lamb (1979). In conventional models, the inner disk radius r_{in} in a steady-state is usually assumed to be equal to r_ξ .

The diffusion timescale of the field lines in the disk is comparable to the viscous timescale which is much longer than the interaction timescale of the field lines and the inner disk, $t_{int} = |\Omega_K - \Omega_*|^{-1}$, (Fromang & Stone 2009) where Ω_* is the angular velocity of the neutron star. The field lines cannot slip through the disk. Theoretical studies and numerical simulations show that the field lines interacting with the inner disk in a narrow boundary inflate and open up within the interaction timescale (Aly 1985, Lovelace et al. 1995, Hayashi et al. 1996, Miller & Stone 1997, Uzdensky et al. 2002, Uzdensky 2004). If the system is in the SP phase, the matter flowing in to the boundary at the innermost region of the disk is expelled from the system along the open field lines. The open lines reconnect on the dynamical timescale, Ω_K^{-1} , and continue to apply torque on the matter until they open up again (Lovelace et al. 1999, Ustyugova et al. 2006). The simulations show that the field lines

outside the interaction boundary are decoupled from the disk. The magnetosphere inside the boundary is the region where the closed field lines and the plasma can rotate together at radius $r_m \simeq r_{in}$. These results indicate that a strong-propeller mechanism could be sustained if the field lines expel the matter from the inner boundary at the same rate as that of the mass-flow from the outer disk. Furthermore, for this strong-propeller phase to be steady, the matter should be accelerated to speeds greater than the escape speed, v_{esc} , within t_{int} . Ertan (2017) showed that the maximum radius at which the strong-propeller condition is satisfied is much smaller than r_A , while the accretion rates estimated for the WP/SP transition in this model seem to be in agreement with the transition properties of tM-SPs (Ertan 2017, 2018). The inner boundary in the spin-up phase is also continuously evacuated, as in the case of strong-propeller, but now due to accretion on to the star. At r_{in} the field lines decelerate and bring the matter into co-rotation within t_{int} in the spin-up phase. In other words, the same equation could determine the inner disk radius in both the strong propeller phase (for $r_{in} > r_{co}$) and the spin-up phase (for $r_{in} < r_{co}$). However, this is not the whole story, since the conditions in the spin-up (SU) phase are rather different, in particular r_A enters the picture (Sections 2.1 - 2.4).

In the model, mass accretion on to the star is allowed (WP and SU phases) when $r_{in} \leq r_{co}$, and the system is in the SP phase (no accretion on to the star) when $r_{in} > r_{co}$ where $r_{co} = (GM/\Omega_*^2)^{1/3}$ is the co-rotation radius at which $\Omega_K = \Omega_*$. For a steady strong-propeller mechanism the field should cut the inner disk at a radius greater than $r_1 = 1.26 r_{co}$, because the field lines inside this radius cannot expel matter from the boundary with speeds greater than v_{esc} . In the WP phase, $r_{in} = r_{co}$ and the mass coupling to the field lines at this radius flows on to the star along the field lines. Below, starting from the source properties in the SP phase (Section 2.1), we describe the variation of the inner disk radius r_{in} with increasing disk mass-flow rate \dot{M}_{in} , leading to the transitions into the WP phase at a certain \dot{M}_{in} (Section 2.2), and into the SU phase at a much higher accretion rate (Section 2.3). The torque calculations are described in Section 2.4.

2.1 Strong-propeller (SP) phase

In this phase, all the mass flowing into the narrow inner boundary region with radial width δr is efficiently thrown out of the system with a rate equal to the rate of mass flow from the outer disk. δr is estimated to be a few disk thickness, much smaller than the r_{in} (Ertan 2018). This boundary region is the continuously evacuated innermost region of the disk. The field lines could interact with the inner disk in a larger region outside the inner boundary with radial thickness Δr that is a small fraction of r_{in} ($\delta r \ll \Delta r < r$). This is likely to result in a flow of matter expelled from the larger boundary back to the disk at larger radii (backflow) in addition to the outflow from the inner boundary (see Fig. 1 in Ertan 2018). In this case, a steady state is reached with a pile-up outside r_{in} , with a net mass-flow rate \dot{M}_{in} into δr at r_{in} equal to the rate of outflow from this region. Continuous interaction of the field lines with the pile-up exerts a spin-down torque on the star that is much greater than the torque associated with the angular momentum loss to the outflowing gas (Ertan 2017).

Through simple analytical calculations, Ertan (2017) showed that the maximum inner disk radius, $r_{in,max}$, at which the strong-propeller mechanism can work is related to the mass-flow rate of the disk \dot{M}_{in} , rotational period P , and the dipole moment μ of the

neutron star through

$$R_{\text{in,max}}^{25/8} \left| 1 - R_{\text{in,max}}^{-3/2} \right| \approx 1.26 \alpha_{-1}^{2/5} M_{1.4}^{-7/6} \dot{M}_{\text{in,16}}^{-7/20} \mu_{30} P^{-13/12} \quad (1)$$

where $R_{\text{in,max}} = r_{\text{in,max}}/r_{\text{co}}$, $M_{1.4} = (M/1.4M_{\odot})$, $\dot{M}_{\text{in,16}} = \dot{M}_{\text{in}}/(10^{16} \text{ g s}^{-1})$, $\mu_{30} = \mu/(10^{30} \text{ G cm}^3)$, α is the α -parameter of the kinematic viscosity (Shakura & Sunyaev, 1973), and $\alpha_{-1} = (\alpha/0.1)$. In the SP phase, the inner disk radius is expected to be close to $r_{\text{in,max}}$ because of the sharp radial dependence of magnetic torques. We define the radii $R_{\eta} = \eta R_{\text{in,max}}$ and $R_{\xi} = \xi R_A = \xi r_A/r_{\text{co}}$. It can be shown that r_{η} is always much smaller than r_A in the SP phase (see equation 9 in Ertan 2017).

The solutions for R_{ξ} (dashed blue curve) and R_{η} (dashed dotted red curve) are given in Fig. (1a) for an illustrative source, a MSP with $P = 5 \text{ ms}$ and $\mu = 10^{26} \text{ G cm}^3$. As we discussed above, the values of both ξ and η are estimated to be close to unity. For the torque variation of PSR J1023+0038, a tMSP, Ertan (2018) obtained reasonable results with $\eta \approx 0.8$. For all calculations, we set $\xi = 0.5$, the value estimated by Ghosh & Lamb (1979) and $\eta = 1.0$. We will also show the effects of these parameters on our results in Section 3. The solid curve shows the variation of the inner disk radius $R_{\text{in}} = r_{\text{in}}/r_{\text{co}}$ (in the direction of the small arrows) with increasing \dot{M}_{in} . The system is in the SP phase for \dot{M}_{in} values up to point B with $R_{\text{in}} = R_{\eta}$. For a given \dot{M}_{in} in this phase, it is seen that r_{η} is always smaller than r_{ξ} . In the conventional models, it is estimated that $r_{\text{in}} = r_{\xi}$, while in our model, $r_{\text{in}} = r_{\eta}$ up to the \dot{M}_{in} that gives $r_{\text{in}} = r_1 = 1.26r_{\text{co}}$. With increasing \dot{M}_{in} beyond this rate, the system enters the weak-propeller regime with a transition from B to D (Fig. 1a). The reasons for this distinction between r_{ξ} and r_{η} are explained in detail by Ertan (2017). The main reason is that all the matter arriving at r_{ξ} cannot be thrown out with speeds greater than v_{esc} . With the resultant pile-up, the inner disk extends toward inner radii opening up the field lines. Both the field strength and t_{int} increases with decreasing radius. If the inward motion of the inner disk is stopped at a radius greater than r_1 , the system settles down to a steady SP regime. This phase could persist for \dot{M}_{in} values up to $\dot{M}_{\text{in}} = \dot{M}_{\text{in}}(r_{\eta} = r_1)$.

2.2 Weak-propeller (WP) phase

With increasing \dot{M}_{in} in the strong-propeller phase, if r_{η} decreases below r_1 the inner disk will move gradually inwards until $r_{\text{in}} = r_{\text{co}}$. When r_{in} is instantaneously between r_{co} and r_1 , the field lines could easily expel matter from the inner boundary because of increasing t_{int} and field strength as r_{in} approaches r_{co} , nevertheless the speed of the outflowing matter cannot exceed v_{esc} . This leads to a growing pile-up outside r_{in} which pushes the inner disk inwards until r_{in} reaches r_{co} (from B to D in Fig. 1a).

We estimate that $r_{\text{in}} = r_{\text{co}}$ persists over a large range of accretion rates (between D and E), because, in addition to long t_{int} in the boundary, viscous stresses are not sufficient for the inner disk to penetrate inside r_{co} as long as r_{ξ} remains outside r_{co} . The matter couples to the field lines at r_{co} and flows on to the star along the field lines. In this phase, the conditions inside r_{co} also force r_{in} to stay close to r_{co} (Section 2.3). We note that this inner disk behavior is similar to that estimated in the trapped disk model (D’Angelo & Spruit 2012). In our model, the condition for the WP/SP transition and the inner disk radius in the SP phase are well defined, and the physical reason for keeping $r_{\text{in}} = r_{\text{co}}$ in the WP phase is different from reasons proposed in other models (see also Section 2.3).

What is the critical accretion rate at which the inner disk can penetrate inside r_{co} ? The viscous stresses dominate the magnetic

stresses above a critical accretion rate corresponding to $r_{\xi} = r_{\text{co}}$ (point E in Fig. 1a). When the mass inflow rate increases above this level the inner disk and the boundary region move inwards. During this transition, if the disk-field interaction region remains narrow, as estimated in the simulations (Lovelace et al. 1995), the field lines should decouple from the disk outside r_{co} . This switches off the magnetic spin-down torque produced by the disk-field interaction, leading to the spin-up phase at higher mass inflow rates. The details of the torque calculation are given in Section 2.4. For a range of parameters, our results indicate that the magnetic spin-down torque dominates the spin-up torque produced by accretion on to the star for the entire WP phase. With the disk parameters used in this model, the spin-up is likely to start when the inner disk enters inside r_{co} , with $r_{\text{in}} = r_{\xi}$ (point E in Fig. 1a). We will show in Sec. 3 that this result is valid not only for the illustrative source seen in Fig. 1a, but also for other systems including strongly magnetized neutron stars with much longer periods, like 4U 1626–67.

2.3 Spin-up (SU) phase

In the SU phase with $R_{\text{in}} < 1$, the field lines at the inner boundary should be sufficiently strong to force the matter into co-rotation, like in the SP phase. In the R_{in} calculation for the SU phase, the only difference compared to the SP case is the sign of $(\Omega_{*} - \Omega_K)$. This expression appears only in the absolute value in the t_{int} term (Ertan 2017). This means that equation (1) represents the solutions for the SU phase ($R_{\text{in}} < 1$) as well.

For \dot{M}_{in} increasing beyond the WP/SU transition rate, it is seen in Fig. 1a that the condition $r_{\text{in}} = r_{\xi}$ persist until R_{ξ} crosses the R_{η} curve (between the points E and F). The R_{η} solution is double valued for the $R_{\eta} < 1$ region. The positively sloped upper branch appears because of increasing t_{int} as r_{η} approaches r_{co} . This branch of the solution is not stable, but has some important indications: Even for high accretion rates, the inner disk matter can easily be brought into co-rotation at radii close to r_{co} in the region between the upper branch of R_{η} and $R_{\text{in}} = 1$ line (Fig. 1a). In this region, the strength of the field lines are more than sufficient to force the inner disk matter into co-rotation. This also guaranties that $r_{\text{in}} = r_{\text{co}}$ in the weak-propeller phase when $r_{\xi} > r_{\text{co}}$. In that case, the high- \dot{M}_{in} part of this region is not physically realizable. For instance, the model source in Fig. 1a can never reach a point that remains in the high- \dot{M}_{in} side of the E-F line in this region, because r_{in} cannot be greater than r_{ξ} where viscous and magnetic stresses are equal. This is also the reason for the source to follow the E-F line with increasing \dot{M}_{in} .

At point F, with a slight increase in the accretion rate, the inner disk encounters a range of radii along which the field lines are not able to bring the matter into co-rotation within t_{int} . This results in an extension of the inner disk inwards, opening the field lines, down to the radius at which the field is strong enough to sustain the co-rotation. This stable radius is achieved on the negatively sloped lower branch of the r_{η} solution at the point corresponding to the same \dot{M}_{in} (point G in Fig. 1a). This inner disk radius is stable, and with further increase in \dot{M}_{in} , the inner disk radius decreases tracking r_{η} .

The points F and G seen in Fig 1a do not correspond to the same R_{in} values for sources with different P and/or μ . For some sources, R_{ξ} could remain below, and never intersects the R_{η} curve. In these cases, the inner disk radius remains equal to r_{ξ} for the entire spin-up phase. These possibilities will be discussed with examples in Section 3. Due to decreasing r_{in} with transition from F to G, the torque decreases on the viscous time-scale. We estimate that

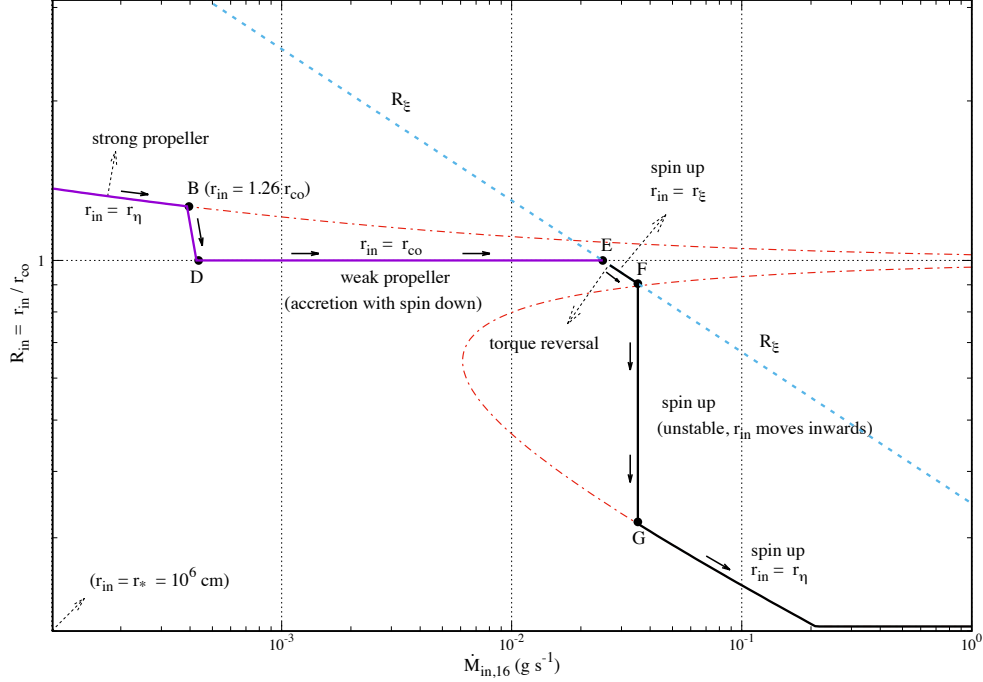


Figure 1a. Variation of r_{in} with \dot{M}_{in} in the strong-propeller phase, the weak-propeller phase, and the spin up phase (solid curve). Small arrows show the variation of r_{in} with increasing \dot{M}_{in} . For this illustrative model, $\Delta r/r_{\text{in}} = 0.2$, $\eta = 1.0$, $\xi = 0.5$, $B = \mu/r_*^3 = 1 \times 10^8$ G, and $P = 5$ ms (see the text for details).

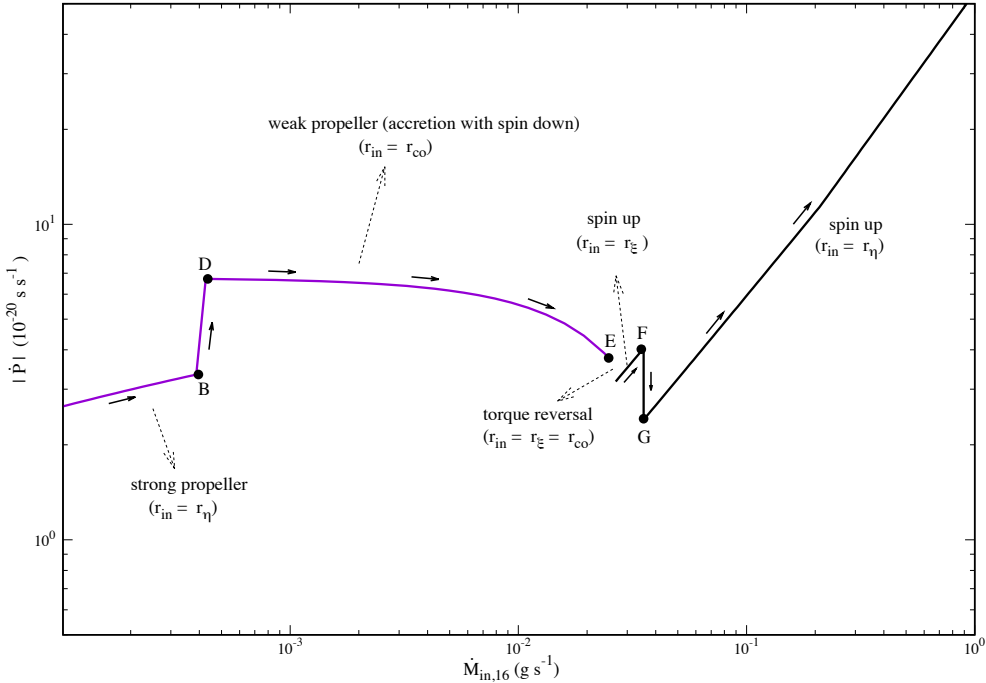


Figure 1b. Variation of \dot{P} with \dot{M}_{in} for the same source given in Fig. 1a. The points with letters corresponds to the points in Fig 1a denoted by the same letters. Note that the source shows a torque reversal around point E with a small variation in \dot{M}_{in} . The transition from B to D corresponds to the WP/SP transition with propagation of the inner disk from r_1 to r_{co} . For the range of \dot{M}_{in} between the points D and E, the system remains in the WP phase with accretion on to the star from $r_{\text{in}} = r_{\text{co}}$ (see the text for details).

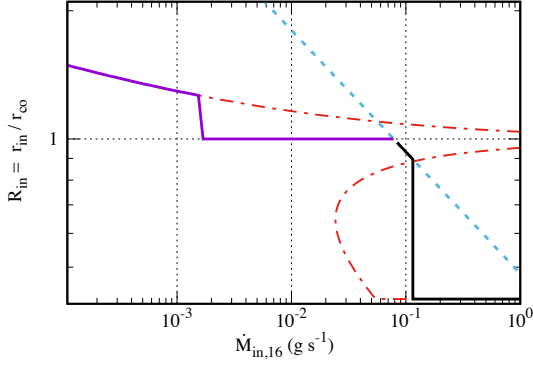


Figure 2a. The same as Fig.1a, but with $B = 5 \times 10^7$ G, $P = 1.69$ ms (properties of PSR J1023+0038).

this sharp torque variation could be observable, if \dot{M}_{in} decreases or increases sufficiently slowly through the rate at point F. For some sources, point G could be found at a radius smaller than the radius of the star, r_* . In this case, when \dot{M}_{in} exceeds the rate at point F, the inner disk extends down to the surface of the star, which is very likely to switch off the pulses produced by the plasma flow channeled by the field lines on to the poles. A model source to illustrate this situation is discussed in Section 3.

2.4 Torques

The total torque acting on the star could be written as the sum of spin-up and the spin-down torques

$$\Gamma = \dot{M}_* (GM r_{\text{in}})^{1/2} - \frac{\mu^2}{r_{\text{in}}^3} \left(\frac{\Delta r}{r_{\text{in}}} \right) + \Gamma_{\text{dip}} \quad (2)$$

The first term is the spin-up torque associated with accretion on to the star from the inner disk. The second term is the magnetic torque arising from the disk-field interaction inside the boundary with radial width Δr . We take $\Delta r/r = 0.2$ in all calculations. Since in all cases we consider here, this magnetic torque dominates the dipole radiation torque, Γ_{dip} , we have ignored Γ_{dip} in our calculations.

In the strong-propeller phase, there is no accretion on to the star, that is, the first term is zero, $r_{\text{in}} = r_{\eta} = \eta r_{\text{in,max}}$. In the weak-propeller phase, both the accretion torque and the magnetic torque act on the star with $r_{\text{in}} = r_{\text{co}}$. In the SU phase, only the accretion torque is active since the inner disk boundary interacting with the field lines is expected to lie inside the co-rotation radius. In this phase, we take $r_{\text{in}} = r_{\xi}$ until r_{ξ} crosses r_{η} (between the points E and F), and $r_{\text{in}} = r_{\eta}$ for the accretion rates greater than the rate at point G (see Fig. 1b).

We obtain the \dot{P} curve given in Fig. 1b for the same source with the \dot{M}_{in} curve given in Fig. 1a. The points corresponding to the same \dot{M}_{in} values in Figs. 1a and 1b are denoted with the same letters. The sharp increase in \dot{P} from B to D is due to the inward motion of the inner disk from $r_1 = 1.26 r_{\text{co}}$ to r_{co} with a slight increase in \dot{M}_{in} when $r_{\text{in}} = r_{\eta} = r_1$ (Section 2.2). With this transition from the SP phase to the WP phase accretion on to the star is switched on.

The system is in the WP regime between points D and E. In this phase, $r_{\text{in}} = r_{\text{co}}$ as explained in Sec. 2.2. The field interacts with the inner disk in the narrow boundary just outside r_{co} , which exerts a spin-down torque on the star. The mass-flow from $r_{\text{in}} = r_{\text{co}}$ along the field lines on to the poles causes a spin-up torque. For the parameters given in Fig. 1a, the spin-down torque dominates the spin-up torque

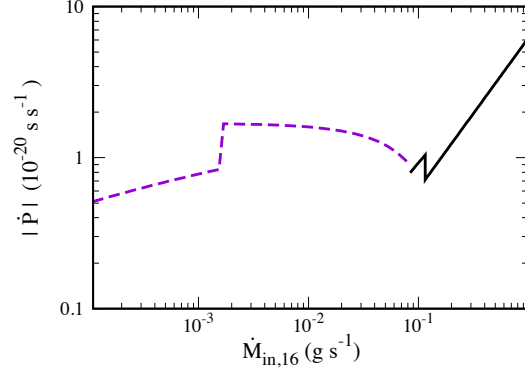


Figure 2b. $|\dot{P}|$ curve for the same source given in Fig 2a.

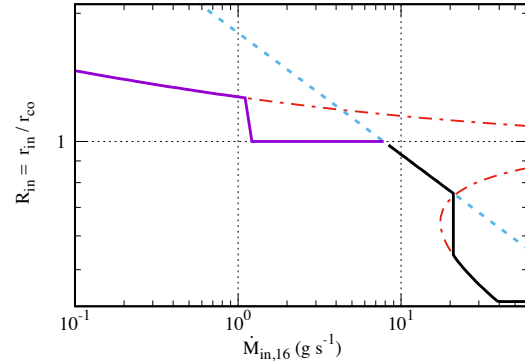


Figure 3a. The same as Fig.2a, but with $B = 5 \times 10^8$ G

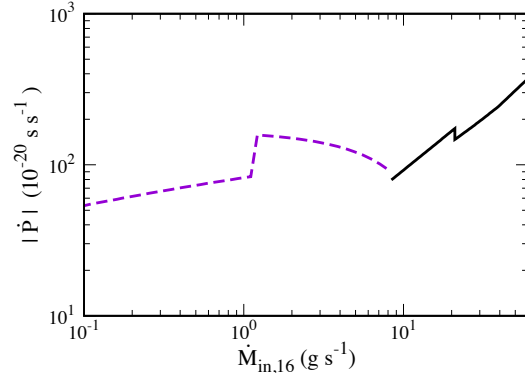


Figure 3b. $|\dot{P}|$ curve for the same source given in Fig 3a.

for the entire WP phase. As seen in Fig. 1b, the magnitude of the spin-down torque is decreasing with increasing \dot{M}_{in} toward the point E. This is because the magnitude of the accretion torque becomes comparable to, while still less than, the magnetic spin-down torque as r_{ξ} approaches r_{co} . In Sec. 3, we also discuss how the features of this transition depend on the chosen parameters $\Delta r/r_{\text{in}}$, η and ξ , as well as μ and P .

The inner disk penetrates inside r_{co} when r_{ξ} becomes smaller than r_{co} , taking the star from the WP to the SU phase. For given μ and P , the critical \dot{M}_{in} corresponding to this transition can be estimated by equating r_{ξ} to r_{co} . The sharp decrease in the magnitude of the torque from F to G corresponds to the propagation of r_{in} from the unstable point F to the stable point G on the lower branch of the r_{η} curve (see Figs. 1a and 1b). With further increase in \dot{M}_{in} , the inner disk radius $r_{\text{in}} = r_{\eta}$ decreases while the magnitude of the spin-up torque increases as seen in Fig. 1b.

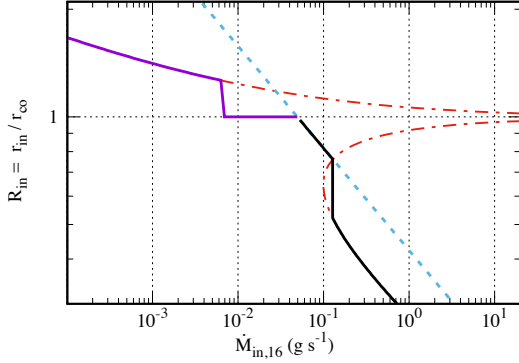


Figure 4a. The same as Fig.1a, but with $B = 1 \times 10^{12}$ G, $P = 10$ s

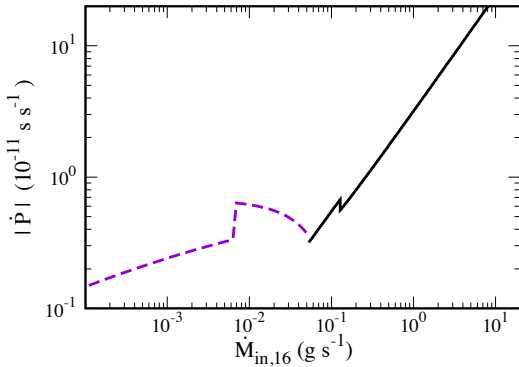


Figure 4b. $|\dot{P}|$ curve for the same source given in Fig 4a.

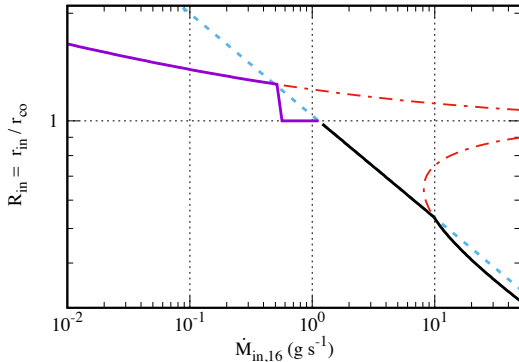


Figure 5a. The same as Fig.1a, but with $B = 3.5 \times 10^{12}$ G, $P = 7.66$ s, the properties of 4U 1626–67

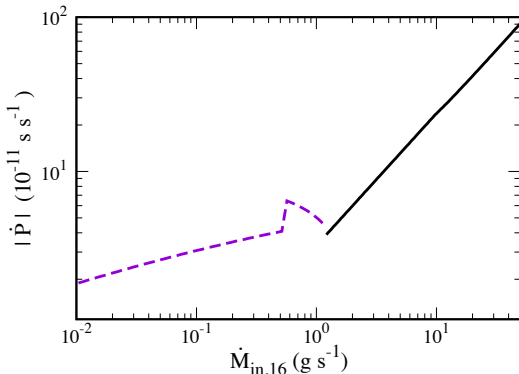


Figure 5b. $|\dot{P}|$ curve for the same source given in Fig 5a.

The model curves given in Figs (1-5) are obtained with the same disk parameters ($\xi, \eta, \Delta r/r_{\text{in}}$). The critical \dot{M}_{in} and r_{in} values corresponding to the SP/WP and torque-reversal transitions change depending on μ and P of the sources. The μ and B values producing the model curves in Figs. (1-3) and Figs. (4-5) are typical values for the millisecond pulsars and LMXBs (or HMXBs) like 4U 1626–67 respectively. Tracing orders of magnitude ranges for μ and/or P values, we always find the same torque-reversal behavior: an abrupt change in the sign of the torque without a significant change in its magnitude occurs with a small change in the mass-flow rate of the disk.

3 DISCUSSION

The model curves seen in Figs. (2 - 5) are obtained with the same set of parameters used for the model given in Fig. 1, except for the $B = \mu/r_*^3$ and P values. For the source seen in Fig. 2, $P = 1.69$ ms and $B = 5 \times 10^7$ G, the properties of tMSP PSR J1023+0038 are employed. In Fig. 2a, it is seen that systems similar to this source are not expected to show pulsations at accretion rates greater than about 10^{15} g s^{-1} . Comparing with Fig. 1a, it is seen in Fig. 2a that the radius at point G is smaller than r_* , indicating that the inner disk extends to the surface of the star. For this source, $r_* = 1 \times 10^6$ cm corresponds to $R_{\text{in}} = 0.42$. This model source shows the WP/SU transition at slightly lower \dot{P} and \dot{M}_{in} values in comparison with the source given in Fig. 1.

For the model curve given in Fig. 3 all the parameters are the same as those given in Fig. 2, except the field strength is increased to $B = 5 \times 10^8$ G, which shifts the critical \dot{M}_{in} values upwards for both the SP/WP transition and the torque reversal. The critical torque reversal rate increases because $r_{\xi} = r_{\text{co}}$ requires a greater \dot{M}_{ξ} for a stronger field ($r_{\xi} \propto B^{4/7} \dot{M}_{\text{in}}^{-2/7}$). The magnitudes of the spin-up and spin-down torques close to the torque reversal also increase with increasing B , while their ratio remains similar. For this case, the crossing point F is at a slightly smaller R_{in} , while the points F and G are closer to the minimum of r_{η} curve.

The source given in Fig. 4, illustrates a strongly magnetized neutron star with $B = 1 \times 10^{12}$ G and $P = 10$ s, parameters typical of HMXBs or LMXBs like 4U 1626–67, and very different from those of the millisecond pulsars discussed above. It is seen, by comparing Figs. 2 and 4, that the torque reversal for these very different systems takes place at similar \dot{M}_{in} , but with orders of magnitude different \dot{P} values. It is very remarkable that the ratios of the of the spin-up and spin-down torque magnitudes across the torque reversals are similar for these rather different model sources.

The model curves in Fig. 5 are produced with the estimated properties of 4U 1626–67, $B = 3.5 \times 10^{12}$ G and $P = 7.66$ s (Giacconi et al. 1972, Orlandini et al. 1998). For this source, the \dot{M}_{in} corresponding to the torque reversal is about 10^{16} g s^{-1} . As seen in Fig. 5b the magnitudes of the spin-up torque and the spin-down torque are similar around the torque reversal with $|\dot{P}| \approx 3 \times 10^{-11} \text{ s}^{-1}$ ($|\dot{\nu}| \approx 5 \times 10^{-13} \text{ Hertz s}^{-1}$). This is consistent with the observed rotational rates of the source during the torque reversals (Camero-Arranz et al. 2010, Chakrabarty et al. 1997a). The torque reversal could occur with a small change in \dot{M}_{in} .

The model parameter η does not affect the WP/SU transition, while it changes the critical \dot{M}_{in} for the SP/WP transition. The model curves seen in Fig. 6 illustrate the effect of η on these transitions. The effects of the parameters ξ and $\Delta r/r_{\text{in}}$ on the ratio of the torque magnitudes during the torque reversals are degenerate. For a smaller $\xi = r_{\xi}/r_A$, the transition takes place at a lower \dot{M}_{in} with a smaller

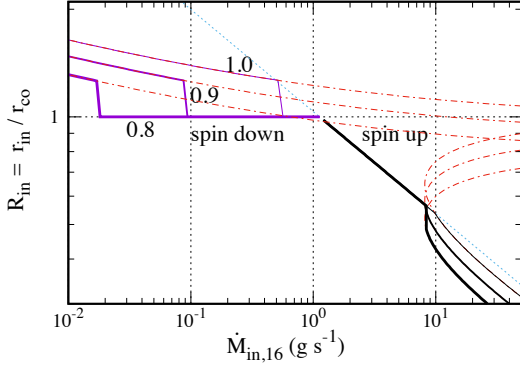


Figure 6a. The same as Fig. 5a, but with different η values seen on the model curves

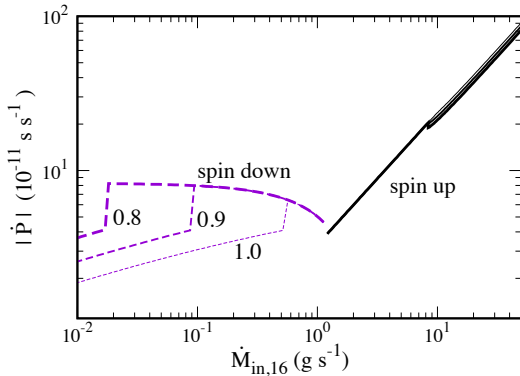


Figure 6b. $|\dot{P}|$ curves for the sources given in Fig 6a.

accretion torque, while a smaller $\Delta r/r_{\text{in}}$ gives a weaker spin-down torque during the torque reversal. To illustrate this effect, we plot the model curve in Fig. 7, using the same parameters of the model curve with $\eta = 0.9$ in Fig. 6, except with a greater ξ parameter ($\xi = 0.7$). As seen in Fig. 7, the torque reversal occurs with increasing \dot{M}_{in} could take place before the inner disk penetrates into r_{co} . Like in the previous examples, torque reversal occurs with a small change in \dot{M}_{in} , and with similar torque magnitudes before and after the torque reversal. In Fig. 8, we plot the torque variations for three different $\Delta r/r_{\text{in}}$ values. It is seen that the spin-down torque is increasing with increasing $\Delta r/r_{\text{in}}$, while the spin-up torque remains constant, since this parameter does not affect the accretion torque.

For the illustrative sources, with different P and μ values, Figs. 1-5 show that transitions occur without significant changes in \dot{M}_{in} and $|\dot{P}|$, which are in agreement with observed torque reversal properties (Section 1). Considering that the disk parameters η , ξ and $\Delta r/r_{\text{in}}$ are roughly similar for different systems, the ratio of the spin-down and spin-up torques across the WP - SU torque reversal transition is expected to be similar for different sources, and for a reasonable set of disk parameters our results indicate that this ratio is likely to be close to unity. The timescale for the torque reversal depends on the rate of change of \dot{M}_{in} during the transition.

When the system is in the weak-propeller phase, small variations in \dot{M}_{in} could lead to occasional transitions between the WP and SP phases with durations in both states much longer than the viscous time-scale of the inner disk. In our model, the \dot{M}_{in} dependence of r_{η} in the strong-propeller phase is much weaker than that of commonly assumed inner disk radius r_{ξ} (see Fig. 1a). This means that once $r_{\text{co}} < r_{\text{in}} < r_1$, it is not easy to refill the inner disk due to this behavior of r_{η} . Both B and t_{int} increases as r_{in} comes

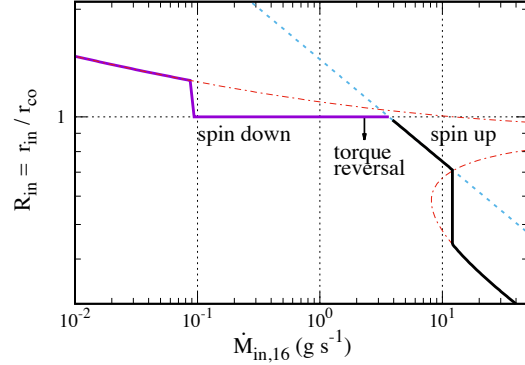


Figure 7a. The same as the curve in Fig. 6 with $\eta = 0.9$, but with $\xi = 0.7$.

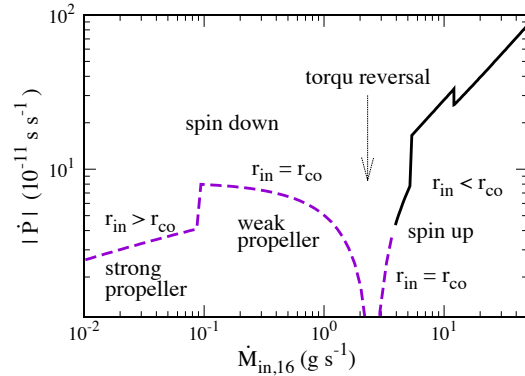


Figure 7b. $|\dot{P}|$ curve for the source given in Fig 7a.

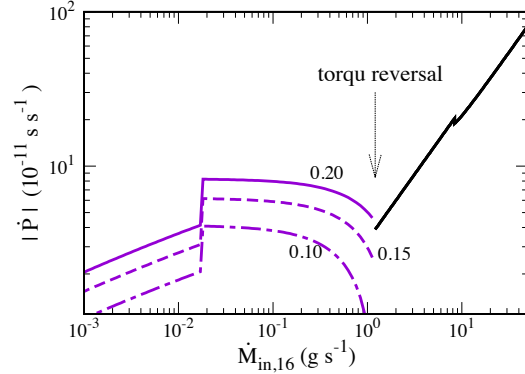


Figure 8. $|\dot{P}|$ curves for different $\Delta r_{\text{in}}/r$ values seen on the model curves for $B = 3.5 \times 10^{12}$ G, $P = 7.66$ s., $\eta = 0.8$

close to r_{co} in the strong-propeller phase. For a steady mass-flow from the outer disk, if $r_{\text{co}} < r_{\text{in}} < r_1$ instantaneously, it is inevitable that r_{in} will decrease, and eventually become equal to r_{co} . This requires a significant growth of the inner pile-up while the matter is being expelled from the inner boundary to larger radii continuously, which could take a time much longer than the viscous time-scale. Note that the weak \dot{M}_{in} dependence of r_{η} also guaranties that r_{in} remains close to r_{co} in this transient strong-propeller phase. The details of these events including recurrence times should be studied through numerical analysis. We note here that these events could lead to transitions between the radio pulsar and the LMXB states, and between the high X-ray modes (X-ray pulsar) and the low X-ray modes (no X-ray pulses) of tMSPs (Ertan 2018).

In the weak-propeller phase, the inner disk is not likely to significantly penetrate inside r_{co} when $R_{\xi} > 1$. Because, in addition

to long t_{int} in the boundary region, the r_{H} solution for the spin-up phase implies that the field lines inside and close to r_{co} can easily bring the matter into co-rotation forcing accretion on to the star from r_{co} for the accretion rates lower than $\dot{M}_{\text{in}}(R_{\xi} = 1)$ (see Section 2). To sum up, in this phase, due to the conditions around r_{co} , the inner disk radius always tends to be very close to r_{co} between the critical accretion rates defined in Section 2. The field lines interacting with the inner disk could produce a continuous backflow of matter from the inner boundary to larger radii, and also injects angular momentum to the pile-up which is the dominant mechanism generating the spin-down torque.

Finally, before and after the transitions from the SU to the WP phase with some rapid changes in the accretion rate, the inner disk may not immediately establish the steady-state conditions. Possibly, there could also be small variations in the geometry of the inner boundary with changing \dot{M}_{in} as well. These effects, which are not addressed in our model, could lead to torque and X-ray luminosity variations in ways different from expected in our model for a particular accretion regime. For instance, the gradual decrease in the spin-down rate of 4U 1626–67 following its transition to the spin-down phase (Chakrabarty et al. 1997a) by $\sim 30\%$ accompanying the decrease in the X-ray flux by a factor of ~ 2 (Camero-Arranz et al. 2010) could be due to these \dot{M}_{in} dependent small variations in the inner boundary. As pointed out by Bildsten et al. (1997), the change in the observed X-ray flux in a particular energy band should also be taken with some caution, considering that it may not reflect the variation in the bolometric luminosity.

Our results in this work are obtained for the neutron stars with geometrically thin, optically thick accretion disks. Wind accretion could significantly change the torques and the critical condition for the torque reversals. In particular, observations indicate a persistent accretion disk in LMXB GX 1+4 (Chakrabarty & Roche 1997). In this wide binary system (Hinkle et al. 2001), Roche-lobe overflow is unlikely. The source of mass-flow on to the neutron star is estimated to be slow stellar wind from the giant companion forming a quasi-spherical accretion geometry (González-Galán et al. 2012) for which the torque-reversal conditions cannot be estimated in our model. Another disk-fed system Cen X-3 (Bildsten et al. 1997) is an HMXB. Its disk is likely to form through Roche-lobe overflow, while the X-rays are estimated to be obscured occasionally by the wind of the companion (Camero-Arranz et al. 2010). Superimposed on a long-term secular spin-up with $\dot{\nu} \sim 8 \times 10^{-13}$ Hz s^{-1} , the source shows rapid transitions between the steady spin-up and spin-down phases lasting 10 - 100 days with average $\dot{\nu}$ magnitudes of $\sim 7 \times 10^{-12}$ Hz s^{-1} and $\sim 3 \times 10^{-12}$ Hz s^{-1} respectively (Bildsten et al. 1997). If the disk-field interaction is the dominant torque mechanism acting on this source, a dipole moment $\mu_{30} \sim 5$ with $\dot{M}_{\text{in}} \approx 1 \times 10^{17}$ g s^{-1} produces a torque reversal in our model consistently with the observed torques. Considering that the wind effect may not be negligible, this result should be taken with some caution.

Observations of 4U 1626–67 clearly showed that the source has a geometrically thin (optically thick) disk before and after the torque reversals (Camero-Arranz et al. 2010). The emission line complex around 1 keV and iron K-fluorescence line at 6.4 keV observed in both the spin-up and the spin down phases show that the temperature of the inner disk environment remained below a few keV, which implies that the optical structure of the disk did not change during the torque reversal (Camero-Arranz et al. 2012). Furthermore, the accretion rates estimated to be greater than about 10^{15} g s^{-1} from the X-ray spectra for the both torque reversals are also in agreement with the presence of a geometrically thin disk around the source

in both spin-up and spin-down. During the torque reversals, there are also systematic changes in the spectra (Camero-Arranz et al. 2012) and pulse profiles that remain stable in the long-lasting spin-up and spin-down phases (Beri et al. 2014). In our model, the inner disk penetrates into r_{co} and propagates inwards after the transition to the spin-up phase. This could result in significant changes in the geometry and optical properties of the accretion column of the star, and thereby, also change the pulse profile, emission area and temperature, while the emission line properties are modified by the newly established conditions at the inner disk. Nevertheless, the details of these variations in the spectra, pulse shapes and the line properties are not addressed in our model.

When this work was in preparation, we noticed the detailed model fits to the torque reversal data of 4U 1626–67 by Benli (2020) assuming $r_{\text{in}} = r_{\text{co}}$ in both spin-up and spin-down phases. The results with this assumption correspond to the particular case in this work given in Fig. 7 for which the inner disk cannot enter inside r_{co} even in the spin-up phase below a critical accretion rate. In our model, with increasing mass-flow rate above this critical level, r_{in} moves inwards as described in Section 2. The results obtained by Benli (2020) seem to favor this torque-reversal behavior. We will perform detailed model fits to the torque reversal data of the sources in an independent work.

4 SUMMARY AND CONCLUSIONS

Extending our earlier work (Ertan 2017, 2018), we have presented a complete picture that could explain the basic properties of neutron stars accreting from geometrically thin accretion disks in the three main states, namely the strong-propeller (SP) phase, the weak-propeller (WP) phase, and the spin-up (SU) phase. In the SP phase, the inner disk radius, r_{in} , is much smaller than the conventional Alfvén radius, r_{A} , and greater than $r_1 = 1.26r_{\text{co}}$. In this phase, all the inflowing disk matter is expelled from the system. The star spins-down by the magnetic torques arising from the disk-field interaction. With increasing \dot{M}_{in} , the system makes a transition from the SP to the WP phase when r_{in} decrease below r_1 , and eventually reaches r_{co} . During this transition, the magnitude of the net spin-down torque decreases due to the contribution of the spin-up torque switched on with the onset of accretion when $r_{\text{in}} = r_{\text{co}}$. In the WP phase, we estimate that most of the inflowing mass is accreted on to the neutron star and the star spins down, since the magnetic torque dominates the spin-up torque for a large range of accretion rates. The inner disk penetrates into r_{co} only when viscous stresses dominate the magnetic stresses at r_{co} , which requires $r_{\xi} = \xi r_{\text{A}} < r_{\text{co}}$. This switches off the magnetic spin-down torque and starts the SU phase. The inner disk with $r_{\text{in}} = r_{\xi}$ during the WP/SU transition, propagates inwards, with increasing accretion rate, to radii smaller than r_{ξ} . Depending on the actual values of inner disk parameters, the torque reversal could take place before the inner disk penetrate into r_{co} (Fig. 7).

The model can account for: (1) accretion on to the neutron star at low X-ray luminosities, (2) transition from the SP to the WP phase at accretion rates much lower than the rates corresponding to the spin-up/spin down transition, (3) ongoing accretion with spin-down over a large range of X-ray luminosity, and (4) torque reversals with comparable torque magnitudes without a significant change in the accretion rate. We have elaborated on this behavior in the context of the tMSPs and extended them to the source 4U 1626-67 which has a much stronger dipole field and a persistent accretion disk, and show torque reversals not affected by the wind of the companion.

There are some other disk-fed LMXB and HMXB systems that show torque reversals with similar properties (Bildsten et al. 1997). Since their torque-luminosity relations are not clear due to either the effect of the wind from the companion or the inconvenient viewing geometry (see Section 1), one can not study their torque-reversal properties. We have presented illustrative model curves for different source properties, which can be tested through future observations of both SP/WP transitions and the torque reversals.

Results of our model calculations indicate that the critical accretion rate corresponding to the torque reversal depends on P and μ of the source. We find that the magnitudes of torques before and after the torque reversal are similar with a ratio that remains almost the same for systems with different P and μ values. Our results also show that the torque reversals could occur without a significant change in the accretion rate independently of the torque-reversal luminosity, period and dipole moment of the sources. In our model, the main reason for the abrupt torque reversal with similar torque ratios is that the inner disk radius is cut at r_{co} in the WP phase, and for the torque model we employ, magnitudes of the net torques in either side of the torque reversal are always found to be similar independent of μ and P (Figs. 1-5). Exact values of the critical \dot{M}_{in} for the torque reversals depend on the actual values of the disk parameters ($\xi, \eta, \Delta r_{\text{in}}/r$). Since these parameters are likely to be similar for different sources, our results imply that the ratios of the spin-up and spin-down torques around the torque reversals are likely to be similar for different neutron stars accreting from geometrically thin accretion disks.

ACKNOWLEDGEMENTS

We acknowledge research support from TÜBİTAK (The Scientific and Technological Research Council of Turkey) through grant 117F144 and from Sabancı University. We thank Ali Alpar for useful comments that have considerably improved the manuscript.

DATA AVAILABILITY

The data underlying this article will be shared on reasonable request to the corresponding author.

REFERENCES

- Aly J. J., 1985, *A&A*, 143, 19
 Arons, J. 1993, *ApJ*, 408, 160
 Archibald, A. M., Stairs, I. H., Ransom, S. M., et al. 2009, *Sci*, 324, 1411
 Bassa, C. G., Patruno, A., Hessels, J. W. T., et al. 2014, *MNRAS*, 441, 1825
 Beri A., Jain C., Paul B., Raichur H., 2014, *MNRAS*, 439, 1940
 Bildsten, L., et al. 1997, *ApJS*, 113, 367
 Camero-Arranz, A., Finger, M. H., Ikhsanov, N. R., Wilson-Hodge, C. A., & Beklen, E. 2010, *ApJ*, 708, 1500
 Camero-Arranz, A., Finger, M. H., Wilson-Hodge, C. A., et al. 2012, *ApJ*, 754, 20
 Chakrabarty, D., & Roche, P., 1997, *ApJ*, 489, 254
 Chakrabarty, D., et al. 1997a, *ApJ*, 474, 414
 Chakrabarty, D., et al. 1997b, *ApJ*, 481, L101
 D’Angelo C. R., Spruit H. C., 2012, *MNRAS*, 420, 416
 Davidson K., Ostriker J. P., 1973, *ApJ*, 179, 585
 Deeter, J. E., Boynton, P. E., Lamb, F. K., & Zylstra, G. 1989, *ApJ*, 336, 376
 Ertan, Ü., 2017, *MNRAS*, 466, 175
 Ertan, Ü., 2018, *MNRAS*, L12, 175
 Fromang S., & Stone J. M., 2009, *A&A*, 507, 19

- Giacconi, R., Murray, S., Gursky, H., Kellogg, E., Schreier, E., & Tananbaum, H. 1972, *ApJ*, 178, 281
 Ghosh, P., & Lamb, F. K., 1979, *ApJ*, 234, 296
 González-Galán, A., Kuulkers, E., Kretschmar, P., et al. 2012, *A&A*, 537, A66
 Hayashi M. R., Shibata K., & Matsumoto R., 1996, *ApJ*, 468, L37
 Hinkle, K. H., Fekel, F. C., Joyce, R. R., Wood, P. R., Smith, V. V., & Lebzelter, T. 2006, *ApJ*, 641, 479
 Illarionov A. F., Sunyaev R. A., 1975, *A&A*, 39, 185
 İnam, S. Ç., Şahiner, S., & Baykal, A., 2009, *MNRAS*, 395, 1015
 Jaodand, A., Archibald, A. M., Hessels, J. W. T., et al. 2016, *ApJ*, 830, 122
 Lamb, F. K., Pethick, C. J., & Pines, D. 1973, *ApJ*, 184, 271
 Lovelace R. V. E., Romanova M. M., & Bisnovaty-Kogan G. S., 1995, *MNRAS*, 275, 244
 Lovelace, R. V. E., Romanova, M. M., & Bisnovaty-Kogan, G. S., 1999, *ApJ* 514, 368
 Miller K. A., & Stone J. M., 1997, *ApJ*, 489, 890
 Orlandini, M., et al. 1998, *ApJ*, 500, L163
 Ostriker, E. C., & Shu, F. H. 1995, *ApJ*, 447, 813
 Papitto, A., Ferrigno, C., Bozzo, E., et al. 2013a, *Natur*, 501, 517
 Papitto A., de Martino D., Belloni T. M., Burgay M., Pellizzoni A., Possenti A., & Torres D. F., 2015, *MNRAS*, 449, L26
 Petterson, J. A., Rothschild, R. E., & Gruber, D. E. 1991, *ApJ*, 378, 696
 Astronomical Society Meeting Abstracts, 223, 140.07
 Shakura, N. I., & Sunyaev, R. A. 1973, *A&A*, 24, 337
 3, 262
 Ustyugova, G. V., Koldoba, A. V., Romanova, M. M., & Lovelace, R. V. E., 2006, *ApJ*, 646, 304
 Uzdensky, D. A., Königl A., & Litwin C., 2002, *ApJ*, 565, 1191
 Uzdensky, D. A., 2004, *Ap&SS*, 292, 573

This paper has been typeset from a \LaTeX file prepared by the author.